



Spray pyrolysis synthesis, electrical and magnetic properties of $\text{Ho}_x\text{Bi}_{1-x}\text{FeO}_3$ nanocrystals

E. V. Tomina^{1,2}, N. A. Kurkin¹, A. K. Korol³, Yu. A. Alekhina³, N. S. Perov³, Fan Jiyu⁴, I. Ya. Mittova¹, Tien A. Nguyen⁵, and Vuong X. Bui^{6,*}

¹Voronezh State University, Voronezh 394018, Russian Federation

²Voronezh State University of Forestry and Technologies Named After G.F. Morozov, Voronezh 394036, Russian Federation

³Lomonosov Moscow State University, Moscow 119991, Russian Federation

⁴Department of Applied Physics, Nanjing University of Aeronautics and Astronautics, Nanjing 210016, China

⁵Ho Chi Minh City University of Education, Ho Chi Minh City 700000, Vietnam

⁶Sai Gon University, Ho Chi Minh City 700000, Vietnam

Received: 24 June 2022

Accepted: 18 September 2022

Published online:

7 October 2022

© The Author(s), under exclusive licence to Springer Science+Business Media, LLC, part of Springer Nature 2022

ABSTRACT

Bismuth ferrite nanopowders doped with holmium ions were synthesized by spray pyrolysis. By means of the TEM and SEM methods, it was established that $\text{Ho}_x\text{Bi}_{1-x}\text{FeO}_3$ particles have dimensions in the range of 50–170 nm and are agglomerated into spherical formations with a size of 1.5–3 μm . A decrease in the lattice parameters and unit cell volume of holmium-doped bismuth ferrite samples was shown, and the EDX data confirm the incorporation of holmium ions into the positions of bismuth ions in the BiFeO_3 lattice. Doping of bismuth ferrite with holmium ions led to a significant increase in the saturation magnetisation and residual magnetisation in comparison with undoped BiFeO_3 , while the coercive force decreased. Magnetic characteristics of $\text{Ho}_x\text{Bi}_{1-x}\text{FeO}_3$ samples demonstrated strong dependence on temperature, and the dielectric permittivity in the frequency range up to 200 kHz remains practically unchanged. Magnetocapacitance values in fields up to 5×10^5 A/m did not exceed a tenth of a percent, which is associated with a high dispersion of nanopowders. The values of M_s and M_r obtained for $\text{Ho}_x\text{Bi}_{1-x}\text{FeO}_3$ open up prospects for using this material for the development of magnetic field sensors, memory cells, and spintronic devices.

1 Introduction

One of the promising areas of modern materials science is the development of synthesis methods, the study of the composition, structure, and possibilities

of using nanosized materials with different functional properties [1–6]. Of greatest interest is bismuth ferrite BiFeO_3 (BFO) which attracts the attention of researchers due to its electrical and magnetic properties. In addition, there are reports on the use of

Address correspondence to E-mail: buixuanvuongsgu@gmail.com

bismuth ferrite nanoparticles in medicine, since they possess antibacterial properties [7].

Out of the whole variety of multiferroics with a perovskite structure, bismuth ferrite is one of the most promising compounds due to the existence of ferroelectric and magnetic phases in it with high ordering temperatures ($T_c = 1083$ K, $T_N = 673$ K [8–11]). This means manifestations of the magneto-electric effect are to be expected at temperatures convenient for practical applications (298 K and higher) and in relatively low fields. However, there are several problems that prevent the realization of the full potential of bismuth ferrite. First, it is quite difficult to obtain single-phase bismuth ferrite. The synthesized samples almost always contain $\text{Bi}_{25}\text{FeO}_{39}$ impurities with a sillenite structure and $\text{Bi}_2\text{Fe}_4\text{O}_9$ with a mullite structure [12–16]. In [17–19], this is explained by thermodynamic reasons associated with the features of the stable existence of BFO, $\text{Bi}_{25}\text{FeO}_{39}$, and $\text{Bi}_2\text{Fe}_4\text{O}_9$. In [20], thermodynamic analysis showed that the regions of stable existence of BFO are below 447 °C and above 767 °C, and, therefore, for the synthesis of pure bismuth ferrite, the process must be carried out in these temperature ranges.

Second, BFO is characterized by a spatially modulated spin structure, which is a cycloid with a period of 62 nm [21]. The spin cycloid is an obstacle to the manifestation of the magneto-electric effect by bismuth ferrite under normal conditions. The reason for the appearance of the cycloid is the inhomogeneous magneto-electric interaction, due to which spontaneous electric polarization induces spatial spin modulation. A change in the degree of polarization will lead to a change in the magnetoelectric interaction and a rearrangement of the spin structure. In the first approximation, the degree of rhombohedral distortion of the cell, c/a , can serve as a criterion for the degree of polarization. The destruction of anti-ferromagnetic cycloid requires changing the c/a ratio, thereby reducing the degree of electric polarization [22].

For BiFeO_3 , various methods of destruction of the spin cycloid are used: the application of a strong magnetic field, the replacement of bismuth ions with ions of rare-earth elements, iron, or other 3d-metals, the production of BiFeO_3 thin films, and others. [22–27]. Rare earth elements as BFO dopants are attractive due to their electronic configuration and the presence of an unfilled 4f shell. In [28], using the example of $\text{R}_{0.15}\text{Bi}_{0.85}\text{FeO}_3$ ($\text{R} = \text{La}, \text{Nd}, \text{Gd}, \text{Dy}, \text{Er}$)

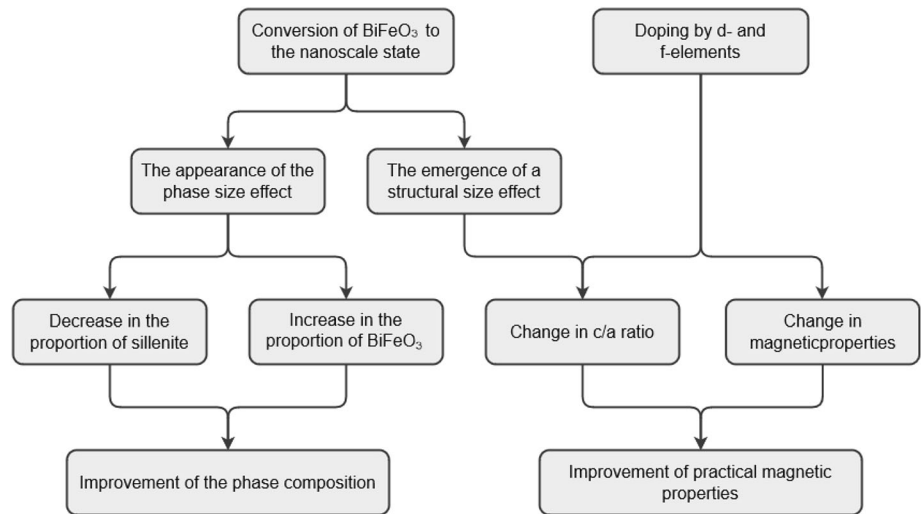
samples it was shown that even small concentrations of introduced rare-earth metal ions significantly changed the magnetic properties of bismuth ferrite. In [29, 30], the doping of BFO with 3d-metals with intrinsic magnetic moments led to an improvement in the magnetic and ferroelectric properties of bismuth ferrite, extended the interval for the formation of continuous solid solutions, and an increase in the thermal stability of BiFeO_3 . It was established in [31] that the doping of BFO with Ni^{2+} ions contributed to an increase in residual magnetisation by 16 times in comparison with undoped bismuth ferrite, which was associated with the superexchange interaction of $\text{Fe}^{3+}\text{-O-Ni}^{2+}$. It was found in [32] that for ceramics of $\text{BiFe}_{0.75}\text{Co}_{0.25}\text{O}_3$ the composition B saturation magnetisation ($M_s = 1.6$ A m²/kg), residual magnetisation ($M_r = 0.7$ A m²/kg), and coercive force ($H_c = 39$ kA/m) increased significantly compared to undoped BiFeO_3 . For BFO nanopowders doped with cobalt ions, the specific magnetisation in a 1.27 MA/m field at a temperature of 100 K was 61.2 A m²/kg and decreased at a temperature of 300 K to 39.5 A m²/kg, nevertheless remaining significantly higher than that for undoped bismuth ferrite [33].

For BiFeO_3 films with a thickness of 50–500 nm, a giant magneto-electric effect (~ 3.8 V/A) was observed at room temperature, exceeding the magneto-electric effects in other materials under the same conditions by several orders of magnitude [34].

In this study, we propose the synthesis of nanoscale BFO with simultaneous doping with ions of the f-block element Ho for the destruction of a spin cycloid (Fig. 1). It is assumed that the transfer of bismuth ferrite into the nanoscale state will entail a change in the ratio of the crystal lattice parameters c/a and, accordingly, a change in the spin structure. A phase size effect is possible, which will lead to a decrease in the content of the low-temperature impurity phase $\text{Bi}_{25}\text{FeO}_{39}$ and an increase in the proportion of the high-temperature phase BiFeO_3 . The difference between the magnetic moments and ionic radii of holmium and bismuth will have a significant effect on the exchange interaction energy and magnetic properties of BFO.

The aim of this study was the synthesis of $\text{Ho}_x\text{Bi}_{1-x}\text{FeO}_3$ nanopowders by spray pyrolysis method and determination of the effect of holmium concentration on the magnetic and electrical characteristics of the samples.

Fig. 1 Proposed approaches to the synthesis of pure BiFeO_3 and destruction of the spin cycloid



2 Experimental

2.1 Materials and methods

Bismuth ferrite samples doped with holmium $\text{Ho}_x\text{Bi}_{1-x}\text{FeO}_3$ (where $x = 0, 0.05, 0.10, 0.15$) were synthesized by the spray pyrolysis method [35]. Crystalline hydrates of holmium nitrate (reagent grade CAS 14483–18-2), iron nitrate (analytical reagent grade TU 6–09-02–553-96), and bismuth nitrate (analytical reagent grade CAS 10035–06-0) in a stoichiometric ratio corresponding to the final composition of $\text{Ho}_x\text{Bi}_{1-x}\text{FeO}_3$ (where $x = 0, 0.05, 0.10, 0.15$) were dissolved in nitric acid with the addition of tartaric acid $\text{C}_4\text{H}_6\text{O}_6$. The solution was placed in the disperser of the BFO synthesis unit (Fig. 2).

In the disperser (2), the solution was transferred to the aerosol state with a particle size of 0.8 to 2.0 μm . Then, the aerosol was transferred by air flow into the reaction chamber (5) and heated in the hottest part to 770 °C. At this temperature, nitrates decompose with the formation of bismuth ferrite. The flow rate was 9 l/min, the aerosol particles were in the reaction zone for about 0.6 s. The particles were collected by passing the gas through water (10). Then, the solution was filtered and the powder was dried in air for 24 h.

2.2 Characterization

The phase composition of the samples was studied using an Empyrean BV X-ray diffractometer with a Cu anode ($\lambda = 1.54060 \text{ nm}$). The start angle was $2\theta = 10^\circ$, the final angle was $2\theta = 80^\circ$, and step = 0.02° . The database of the International Center for

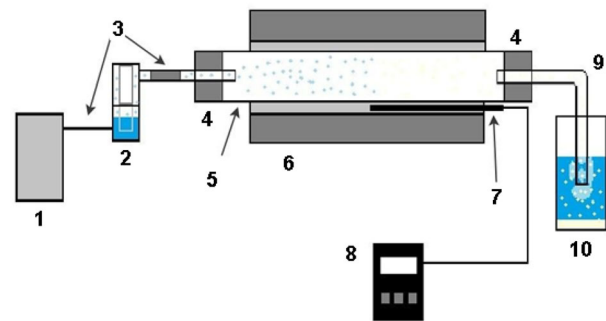


Fig. 2 Scheme of the installation for the synthesis of BiFeO_3 using the spray pyrolysis method. 1 – compressor, 2 – disperser, 3 – nozzles, 4 – rubber stopper, 5 – reactor (quartz tube), 6 –MTP-2 M tube furnace, 7 – thermocouple, 8 – thermostat, 9 – glass tube with 90° turn, 10 – receiver for collecting nanopowder

Diffraction Data (JCPDS) was used for the analysis of diffraction patterns (Cards: 73–0548, 46–0416, 72–1832, 77–2008, 83–0410, 74–2352, 77–2355, 82–1533, 84–0311, 83–0932).

Quantitative elemental analysis and determination of morphological features were carried out on a JSM-6380LV JEOL scanning electron microscope with an INCA 250 microanalysis system. The particle size distribution histogram was plotted using the “ImageJ” program, version 1.53 k.

The particle size was determined by transmission electron microscopy (TEM, transmission electron microscope CarlZeiss Libra-120).

The magnetic characteristics of the samples were measured using a LakeShore 7407 vibrating sample magnetometer in the magnetic fields up to $1.27 \times 10^6 \text{ A/m}$. The powder with mass 20–40 mg was packed in the flat plastic bag. Magnetic moment was

normalized to the mass of the samples, and saturation magnetization (M_s) was obtained after fitting of the high-field region of $M(H)$ curve.

Flat disks with a diameter of 6.1 mm and a thickness of 0.8 mm were made from $\text{Ho}_x\text{Bi}_{1-x}\text{FeO}_3$ samples for measurements of the magnetodielectric effect. The samples were prepared by pressing the initial powder in a mold with a force of 3×10^4 N. The thickness of the samples obtained was determined by the mass of the loaded powder. Electrodes made of the electrically conductive adhesive “Kon-taktol” based on silver were applied on the samples and connected to AM-3016 RLC meter (AKTAKOM). The samples were placed between the poles of an electromagnet that created an external magnetic field in two orientations: along the disk plane and perpendicular to it. The values of the magnetic field were determined using an RSH1-10 magnetic induction meter.

3 Results and discussion

3.1 Phase composition of the synthesized samples

According to XRD data (Fig. 3), BiFeO_3 and $\text{Ho}_{0.05}\text{Bi}_{0.95}\text{FeO}_3$ samples synthesized by spray pyrolysis were almost single phase with an insignificant content of $\text{Bi}_{25}\text{FeO}_{39}$ and $\text{Bi}_2\text{Fe}_4\text{O}_9$. Several reflections of ferrite with a mullite structure were clearly expressed on the diffraction pattern of the $\text{Ho}_{0.15}\text{Bi}_{0.85}\text{FeO}_3$ sample, although they had low intensity. Thus, the

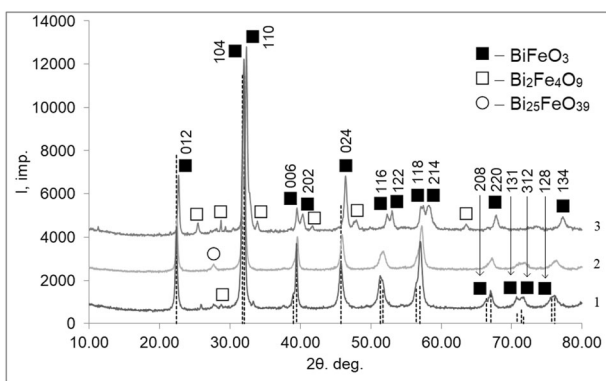


Fig. 3 Diffraction patterns of powders synthesized by spray pyrolysis: 1- BiFeO_3 , 2— $\text{Ho}_{0.05}\text{Bi}_{0.95}\text{FeO}_3$, 3— $\text{Ho}_{0.15}\text{Bi}_{0.85}\text{FeO}_3$. The dashed line indicates the BiFeO_3 standard (Card 73–548)

nominal degree of doping $x = 0.15$ can be considered as the limiting boundary for the introduction of holmium ions into BFO when the content of $\text{Bi}_{25}\text{FeO}_{39}$ and $\text{Bi}_2\text{Fe}_4\text{O}_9$ impurity phases becomes significant.

For the assessment of the content of impurities in the samples (Table 1), a semi-quantitative analysis of diffraction patterns was carried out by the “corundum number” method [36] using the formula

$$w_k = \frac{I_k^{\max} / \text{RIR}_k}{\sum_i I_i^{\max} / \text{RIR}_i}, \tag{1}$$

where w_k is the mass fraction of phase k , I_k^{\max} is the intensity of the largest reflex of the phase k , RIR_k —corundum number of phase k , I_i^{\max} are the intensities of the largest reflections of i phases, and RIR_i are corundum numbers of i phases. The synthesized samples contain less impurities in comparison with the results of other authors [11].

When superimposing diffraction patterns (Fig. 3), a shift in the reflections of samples doped with holmium $\text{Ho}_{0.05}\text{Bi}_{0.95}\text{FeO}_3$ and $\text{Ho}_{0.15}\text{Bi}_{0.85}\text{FeO}_3$, relative to the dopant-free BiFeO_3 , toward higher values of 2θ angles was noted. This finding indicates the distortion of the crystal lattice due to the introduction of ions with other ionic radii. Based on the values of ionic radii ($r(\text{Bi}^{3+}) = 0.117$ nm; $r(\text{Ho}^{3+}) = 0.104$ nm; $r(\text{Fe}^{3+}) = 0.069$ nm; $r(\text{O}^{2-}) = 0.138$ nm); [37] and data on the shift of peaks in the diffraction pattern, it can be concluded that holmium ions were incorporated in the positions of bismuth ions in the crystal lattice of bismuth ferrite.

EDX analysis confirmed the presence of holmium in the samples (Fig. 4 a, b). The average values of the weight percent and atomic percent of the Ho, Bi, Fe, and O elements are shown in Table 2, and the results were consistent with the expected chemical composition (Table 2).

The values of coherent scattering regions (CSR) of the particles of the synthesized samples (Table 3) were calculated using the Scherrer formula [38]:

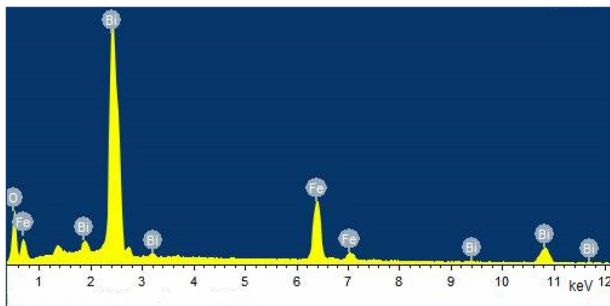
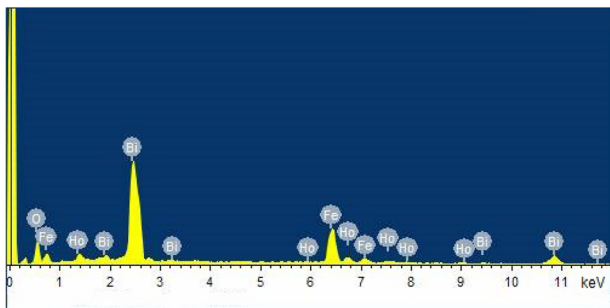
$$\beta = \frac{m\lambda}{D \cos \theta}, \tag{2}$$

where β is the physical broadening, rad; $m = 1$; λ is the wavelength of X-ray radiation, nm; and D is the particle diameter.

As can be seen from Table 3, the average CSR values practically coincided for the undoped BFO and $\text{Ho}_{0.05}\text{Bi}_{0.95}\text{FeO}_3$ samples, taking into account the error. During the transition from $\text{Ho}_{0.05}\text{Bi}_{0.95}\text{FeO}_3$ to

Table 1 Composition of the synthesized bismuth ferrite samples calculated by the corundum number method

	Spray pyrolysis		
	BiFeO ₃	Ho _{0.05} Bi _{0.95} FeO ₃	Ho _{0.15} Bi _{0.85} FeO ₃
Intensity of BiFeO ₃ peak, rel. units	100.0	100.0	100.0
Intensity of Bi ₂₅ FeO ₃₉ peak, rel. units	1.8	3.7	1.3
Intensity of Bi ₂ Fe ₄ O ₉ peak, rel. units	2.7	0	5.9
Content of BiFeO ₃ , % wt	93.0%	94.8%	88.8%
Content of Bi ₂₅ FeO ₃₉ , % wt	2.5%	5.2%	1.7%
Content of Bi ₂ Fe ₄ O ₉ , % wt	4.5%	0.0%	9.5%

**(a)****(b)****Fig. 4** Spectra of elemental composition of samples; **a** – BiFeO₃, **b** – Ho_{0.15}Bi_{0.85}FeO₃**Table 2** EDX analysis of BiFeO₃:Ho³⁺ nanosized powders

Samples	Bi		Fe		O		Ho	
	Wt%	At%	Wt%	At%	Wt%	At%	Wt%	At%
BiFeO ₃	65.52	19.26	18.86	20.74	15.62	60.00	-	-
Ho _{0.05} Bi _{0.95} FeO ₃	63.67	18.94	18.26	20.33	15.37	59.71	2.72	1.02
Ho _{0.15} Bi _{0.85} FeO ₃	57.43	16.74	18.99	20.72	15.62	59.48	7.96	2.94

Table 3 The average CSR of the synthesized samples

The CSR diameter of the particles, nm	BiFeO ₃	Ho _{0.05} Bi _{0.95} FeO ₃	Ho _{0.15} Bi _{0.85} FeO ₃
D ₁	24 ± 2	26 ± 3	28 ± 3
D ₂	17 ± 2	18 ± 2	23 ± 2
D ₃	15 ± 1	15 ± 1	20 ± 2
D _{av}	19 ± 2	20 ± 2	24 ± 3

Ho_{0.15}Bi_{0.85}FeO₃, there was a tendency for a slight increase in CSR values, which may be due to the phase inhomogeneity of the sample due to the presence of Bi₂₅FeO₃₉ and Bi₂Fe₄O₉ impurities in the amount more than 10 wt%.

The lattice parameters of the samples were calculated using the UnitCell program: The calculated data for hexagonal packing are shown in Table 4.

It can be seen that the lattice parameters and its volume decreased with an increased concentration of dopant, which correlated with shift of diffraction angles toward larger values observed in the diffraction patterns of Ho_xBi_{1-x}FeO₃ samples. In general, these data confirmed the incorporation of an ion with a smaller ionic radius (i.e., holmium) in place of an ion with a larger ionic radius (i.e., bismuth). The dependence of the lattice parameters on the degree of doping is satisfactorily approximated by a linear function (Fig. 5).

For the evaluation of possible stoichiometric deviations of the synthesized samples from the nominal composition for the Ho_{0.15}Bi_{0.85}FeO₃ sample, ele-

Table 4 Lattice parameters of BiFeO₃:Ho³⁺ samples synthesized by spray pyrolysis

Lattice parameters	Reference, BiFeO ₃ Card 73–0548	BiFeO ₃	Ho _{0.05} Bi _{0.95} FeO ₃	Ho _{0.15} Bi _{0.85} FeO ₃
a, Å	5.58	5.58	5.56	5.46
c, Å	13.9	13.81	13.79	13.75
V, Å ³	374.81	372.78	369.36	354.84

mental analysis was performed and the real composition was established—Ho_{0.14}Bi_{0.81}FeO_{2.87}. Deviation from the nominal composition can be associated both with the presence of impurities in the sample and with the volatility of bismuth oxide at high temperatures.

3.1.1 Morphological characteristics of particles

The synthesized bismuth ferrite powder is represented by predominantly spherical agglomerates with a size of 1–3 μm (Fig. 6a).

According to TEM data (Fig. 6), agglomerates were formed by particles with a size of 50–170 nm. A significant difference from the CSR values, calculated

using the Scherrer formula, was due to possible significant calculation errors.

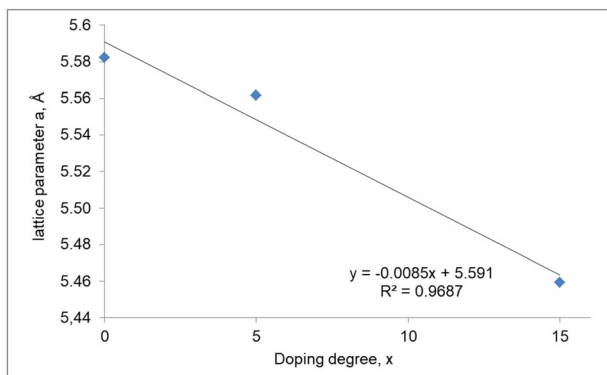
3.2 Magnetic properties of samples

For all synthesized samples, hysteresis loops were measured at temperatures of 300 K and 100 K, according to the obtained dependences of the specific magnetic moment on the magnetic field strength (Fig. 7a, b). The measurements were carried out over a range of fields from -1.27×10^6 A/m up to $+1.27 \times 10^6$ A/m. An external field was applied in the sample plane to minimize the effect of the demagnetising factor.

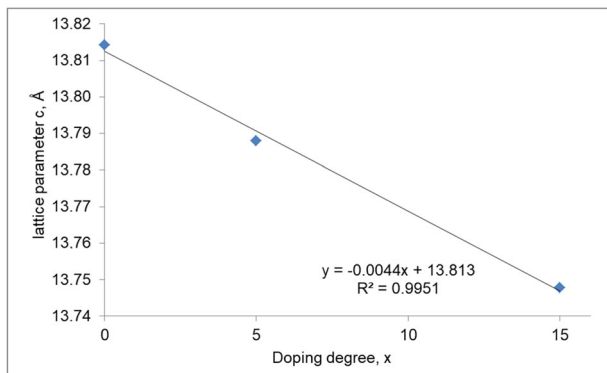
Undoped BiFeO₃ demonstrated a close to linear dependence of the specific magnetic moment on the external field, typical for antiferromagnets, while samples doped with holmium were characterized not only by a higher value of the specific magnetic moment at the same fields, but also by a hysteresis field dependence, which is typical for ferrimagnets (Table 5).

The specific residual magnetisation and specific saturation magnetisation of both pure bismuth ferrite and BiFeO₃ samples, doped with holmium, decreased with an increase in temperature from 100 to 300 K. The coercive force of all samples also decreased with increase in temperature up to 300 K, since thermal fluctuations which “loosen” the spins increase with the increasing temperature and the magnetic order decreases. This type of field dependence of the specific magnetic moment is characteristic of ferrites doped with rare-earth elements [39, 40], as well as rare-earth metal ferrites [41, 42].

At a temperature of 100 K, the values of the specific residual magnetisation and specific saturation magnetisation of Ho_xBi_{1-x}FeO₃ samples naturally increased with an increase in dopant concentration. At 300 K, the trend toward an increase in these characteristics also remained; however, for a sample containing 15% holmium, a slight decrease in M_s compared to that for Ho_{0.1}Bi_{0.9}FeO₃ was observed.



(a)



(b)

Fig. 5 Graph of the dependence of lattice parameter a (a) and lattice parameter c (b) versus doping degree

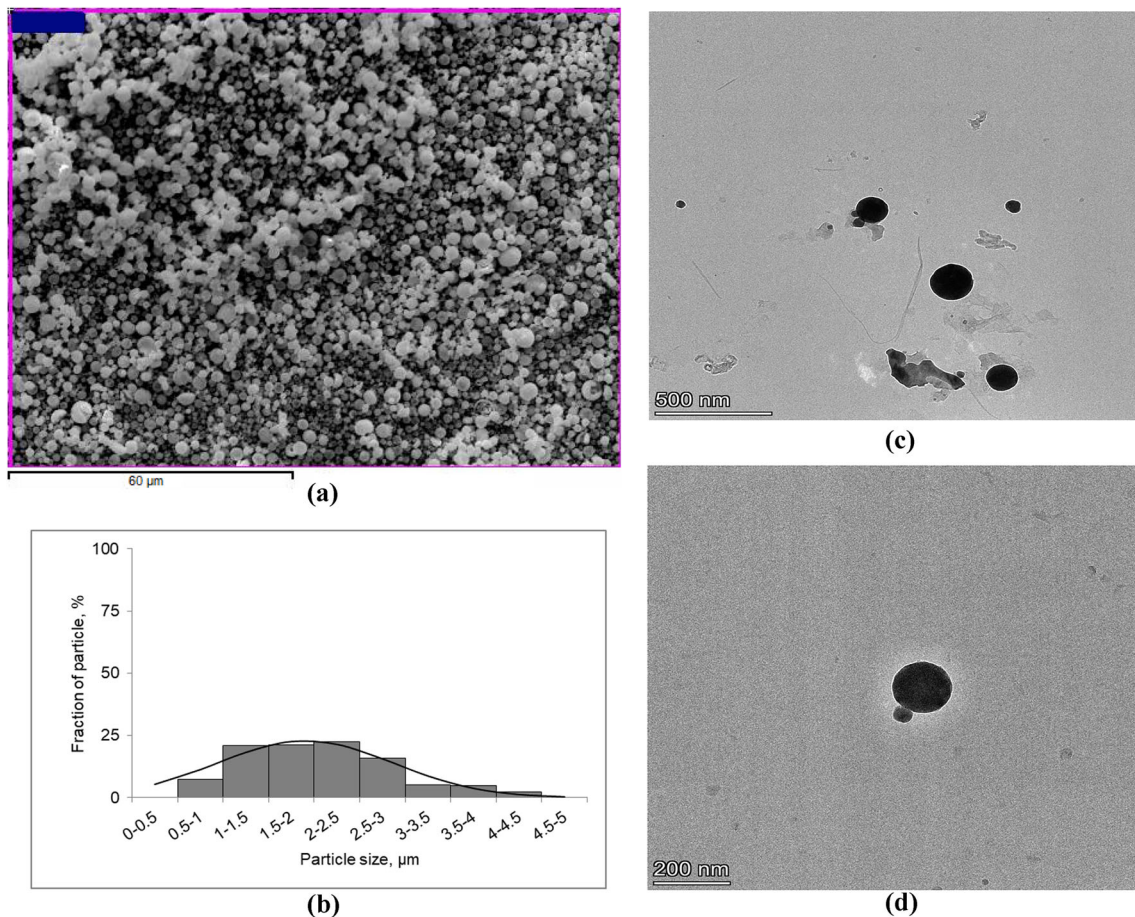


Fig. 6 SEM images of the BiFeO₃ nanopowder (a) and histogram of size distribution of agglomerates (b), TEM image of the BiFeO₃ (c, d)

The decrease in the coercive force with an increase in dopant concentration was clearly expressed; however, the Ho_{0.15}Bi_{0.85}FeO₃ sample both at 100 and at 300 K showed a significant increase in H_c in comparison with undoped bismuth ferrite.

Temperature dependence of the specific magnetic moment in a 1.27×10^6 A/m field is shown in Fig. 8.

For all samples, the specific magnetic moment decreased with an increase in temperature. In this case, with an increase in the holmium concentration to 10%, the curves of the temperature dependence were higher, while the curve of the temperature dependence of the specific magnetic moment for Ho_{0.15}Bi_{0.85}FeO₃ sample was below that for Ho_{0.1}Bi_{0.9}FeO₃.

All revealed dependences of the magnetic characteristics of Ho_xBi_{1-x}FeO₃ samples on the concentration of holmium ions were primarily associated with a

change in the energy of the exchange interaction caused by a change in the parameters of crystal cells due to the difference in ionic radii and magnetic moments of the cations of the substituted bismuth and the substituting holmium. The general trend in the change in the magnetic characteristics of doped bismuth ferrite was impaired at the critical value of the concentration of holmium ions in the range from 10 to 15%. This was also confirmed by the high value of the specific magnetic moment of the Ho_{0.1}Bi_{0.9}FeO₃ sample at all temperatures compared to that for Ho_{0.15}Bi_{0.85}FeO₃ (Fig. 8).

ZFC and FC dependencies were measured in a 3.2×10^4 A/m field for the Ho_{0.15}Bi_{0.85}FeO₃ sample (Fig. 9).

These dependences allowed calculating the average and maximum particle sizes of the sample using

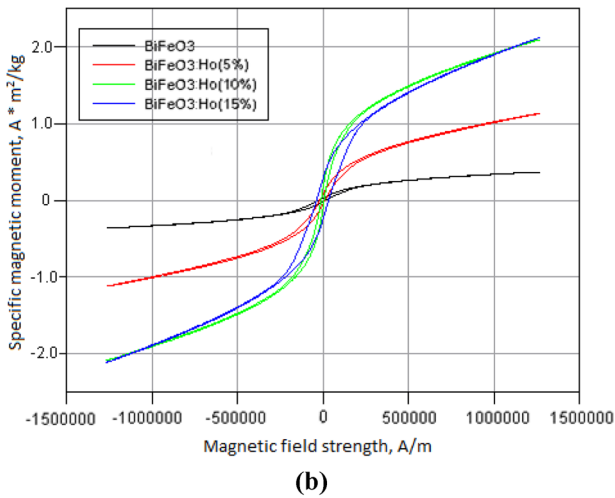
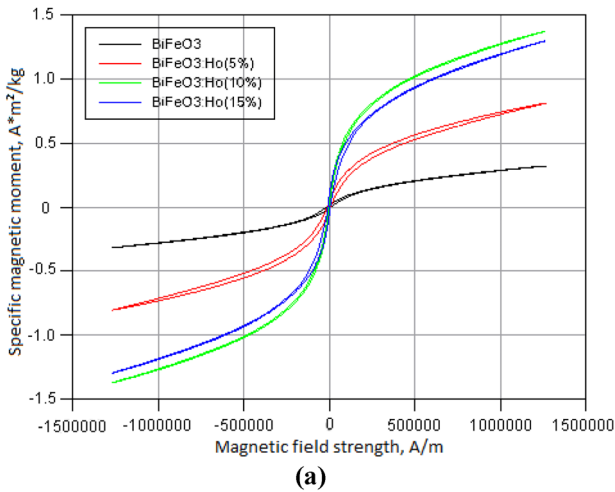


Fig. 7 Hysteresis loops of samples at temperatures of 300 K (a) and 100 K (b)

the Bean-Levenston formulas (3) [43], assuming, according to [44], that for bismuth ferrite $K = 10^5 \frac{erg}{cm^2}$

$$\langle K \rangle \langle V \rangle = KT_f \tag{3}$$

$$\langle K \rangle V_{max} = KT_{rev} \tag{4}$$

Table 5 Results of measurements of magnetic properties of samples

	T = 300 K			T = 100 K		
	H_c , kA/m	M_s , A·m ² /kg	M_r , A·m ² /kg	H_c , kA/m	M_s , A·m ² /kg	M_r , A·m ² /kg
BiFeO ₃	14.3	0.32	0.01	20.8	0.37	0.03
Ho _{0.05} Bi _{0.95} FeO ₃	12.1	0.81	0.04	17.1	1.13	0.07
Ho _{0.1} Bi _{0.9} FeO ₃	2.1	1.37	0.03	10.0	2.09	0.15
Ho _{0.15} Bi _{0.85} FeO ₃	7.5	1.30	0.08	36.0	2.12	0.28

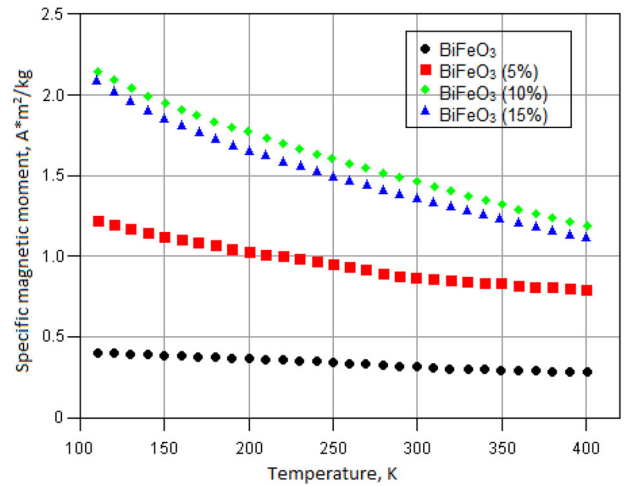


Fig. 8 Temperature dependence of the specific magnetic moment of samples in a 1.27×10^6 A/m field

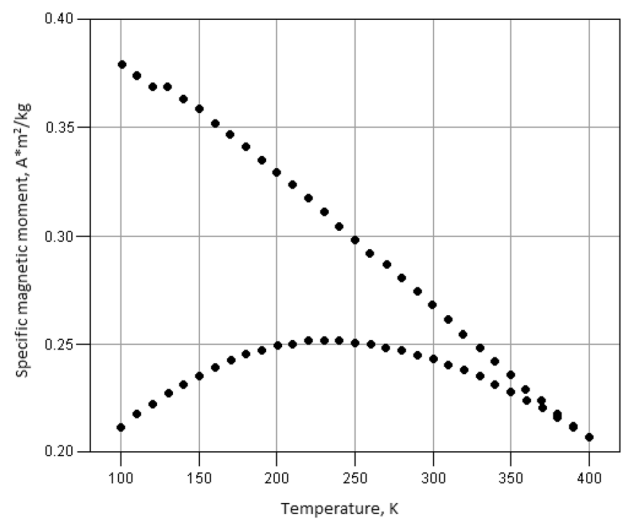


Fig. 9 Temperature ZFC and FC dependences of the Ho_{0.15}Bi_{0.85}FeO₃ sample in a 3.2×10^4 A/m field

where $\langle K \rangle$ is average value of the constant of magnetic crystallographic anisotropy, $\langle V \rangle$ is the average value of the particle volume, K is the Boltzmann constant, T_f is freezing temperature (maximum of ZFC-curve), V_{\max} is the maximum value of the volume of particles, and T_{rev} is the temperature at which the ZFC and FC curves begin to diverge (determined as the temperature at which the difference between the ZFC and FC curves exceeds 3%).

The obtained values of the average particle size of 6.8 ± 0.2 nm and the maximum particle size of 7.8 ± 0.3 nm differ significantly from the results of electron microscopy, which was probably due to the agglomeration of individual nanoparticles into micron objects.

3.2.1 Electrical properties of samples

For measurements of the magnetodielectric effect, the samples were made in the form of flat capacitors, as described above, and connected to an RLC meter to determine the electric capacitance. Using the known values of the electric capacitance and the thickness

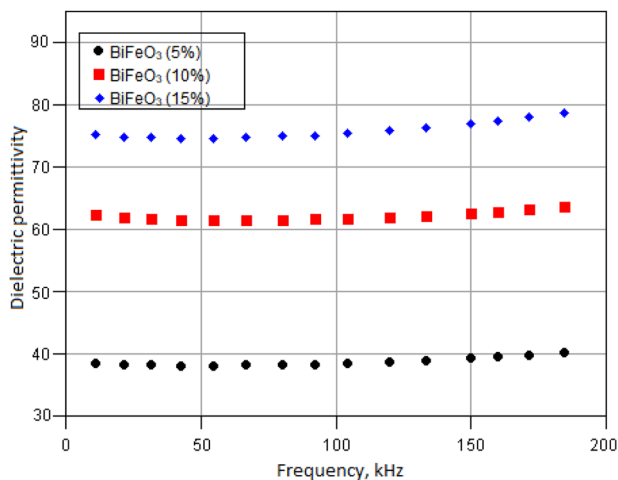


Fig. 10 Dependence of the dielectric permittivity of the samples on the signal frequency

Table 6 Magnetic capacitance values for holmium-substituted ferrites in a magnetic field of 0.4 MA/m at room temperature

Sample	ϵ	$\Delta\epsilon/\epsilon$, %	
		Magnetic field in the sample plane	Magnetic field perpendicular to the sample plane
$\text{Ho}_{0.05}\text{Bi}_{0.95}\text{FeO}_3$	38	-0.010 ± 0.020	-0.015 ± 0.020
$\text{Ho}_{0.1}\text{Bi}_{0.9}\text{FeO}_3$	61	-0.038 ± 0.025	-0.012 ± 0.025
$\text{Ho}_{0.15}\text{Bi}_{0.85}\text{FeO}_3$	76	-0.010 ± 0.015	-0.006 ± 0.015

and area of the capacitor plates, the dielectric constant was calculated using formula (5):

$$\epsilon = \frac{C_d}{\epsilon_0 S} \quad (5)$$

For $\text{Ho}_x\text{Bi}_{1-x}\text{FeO}_3$ samples in the frequency range from 0 to 200 kHz, the dependence of the dielectric permittivity on frequency in a zero external magnetic field was practically absent (Fig. 10), which is consistent with the results of [45] and [46].

Despite the fact, that dependence on the external magnetic field was revealed, it was comparable with the measurement error. At a frequency of 100 kHz at room temperature, the field dependences of the longitudinal and transverse magnetic capacitances of the samples were measured; the results for the maximum field are shown in Table 6.

For this series of samples, the value of the magnetocapacitance was less than a tenth of a percent in any fields and for any orientation of the sample, which disagrees with the results of [47, 48], where the value of the magnetocapacitance was 1% in a field of 1.1 T for pure BiFeO_3 and 1.6% in the field of 1.1 T for $\text{Bi}_{0.95}\text{La}_{0.05}\text{FeO}_3$ and for $\text{Bi}_{0.95}\text{Nd}_{0.05}\text{FeO}_3$. It should be noted that the values given in [47] and [48] were obtained for ceramic BiFeO_3 samples, and therefore, the fact of a strong influence of particle dispersion on the dielectric properties was confirmed.

4 Conclusions

$\text{Ho}_x\text{Bi}_{1-x}\text{FeO}_3$ nanopowders synthesized by spray pyrolysis, according to TEM and SEM, were spherical agglomerates with a size of 1.5–3 μm consisting of individual particles with a size of 50–170 nm. A decrease in the lattice parameters and unit cell volume of the $\text{Ho}_x\text{Bi}_{1-x}\text{FeO}_3$ samples was shown, and EDX data indicate the inclusion of holmium ions in the positions of bismuth ions in the BiFeO_3 lattice. Doping of nanoscale BFO with holmium led to a significant increase in the saturation magnetization

and remanent magnetization, while the coercive force decreases. The magnetic properties of $\text{Ho}_x\text{Bi}_{1-x}\text{FeO}_3$ were characterized by a strong temperature dependence, and the frequency dependence of the permittivity was not observed in the frequency range up to 200 kHz. The values of magnetic capacitance in fields up to 5×10^5 A/m were less than a tenth of a percent due to the high dispersion of particles.

Acknowledgements

The research results were partially obtained using the equipment of the Center for Collective Use of Scientific Equipment of Voronezh State University. URL: <http://ckp.vsu.ru>. The authors acknowledge (partial) support from M.V. Lomonosov Moscow State University Program of Development.

Author contributions

Organization and management, conceptualization, methodology, and formal analysis—EVT; synthesis of samples, analysis of XRD, EDX, TEM, and SEM data—NAK; research and analysis of magnetic and electrical properties of samples—AKK, YAA, and NSP; writing and original draft preparation—NAK, and AKK; writing review and editing—EVT, NSP, FJ, TAN, and IYM; VBX. All authors have read and agreed to the published version of the manuscript.

Funding

The authors declare that no funds, grants, or other support were received during the preparation of this manuscript.

Data availability

The data that support the findings of this study are available from the corresponding author upon reasonable request.

Declarations

Conflict of interest The authors maintain that they have no conflict of interest to be described in this communication.

References

1. R.S. Priya, P. Chaudhary, E.R. Kumar, A. Balamurugan, Ch. Srinivas, G. Prasad, M. Deepty, V. Praveenkumar, B.C. Yadav, D.L. Sastry, Y. Al-Douri, Effect of heat treatment on structural, morphological, dielectric and magnetic properties of Mg–Zn ferrite nanoparticles. *Ceram. Int.* **48**(11), 15243–15251 (2022)
2. K.M. Batoor, E.H. Raslan, Y. Yang, S.F. Adil, M. Khan, A. Imran, Y. Al-Douri, Structural, dielectric and low temperature magnetic response of Zn doped cobalt ferrite nanoparticles. *AIP Adv.* **9**, 055202 (2019)
3. A. Rais, K. Taibi, A. Addou, A. Zanoun, Y. Al-Douri, Copper substitution effect on the structural properties of nickel ferrites. *Ceram. Int.* **40**(9), 14413–14419 (2014)
4. H. Liang, H. Xing, M. Qin, H. Wu, Bamboo-like short carbon fibers@ Fe_3O_4 @phenolic resin and honeycomb-like short carbon fibers@ Fe_3O_4 @FeO composites as high-performance electromagnetic wave absorbing materials. *Composites A* **135**, 105959(2020)
5. H. Liang, H. Xing, Z. Ma, H. Wu, Tailoring high-electroconductivity carbon cloth coated by nickel cobaltate/nickel oxide: A case of transition from microwave shielding to absorption. *Carbon* **183**, 138–149 (2021)
6. Y. Al-Douri, M.O.P. Technologies, *Fundamentals, Processing Methods and Applications* (Elsevier, Amsterdam, 2020), pp.1–401
7. M. Sharmila, R.J. Mani, C. Parvathiraja, S.M.A. Kader, M.R. Siddiqui, S.M. Wabaidur, M.A. Islam, W.-C. Lai, Visible Light Photocatalyst and Antibacterial Activity of BFO (Bismuth Ferrite) Nanoparticles from Honey. *Water* **14**(10), 1545 (2022)
8. Z. Lin, W. Cai, W. Jiang, C. Fu, C. Li, Y. Song, Effects of annealing temperature on the microstructure, optical, ferroelectric and photovoltaic properties of BiFeO_3 thin films prepared by sol–gel method. *Ceram. Int.* **39**(8), 8729–8736 (2013)
9. J. Schell, M. Schmuck, İ Efe, T.T. Dang, J.N. Gonçalves, D. Lewin, M.E. Castillo, V.V. Shvartsman, Â.R.G. Costa, U. Köster, R. Vianden, C. Noll, D.C. Lupascu, Strong magnetoelectric coupling at an atomic nonmagnetic electromagnetic probe in bismuth ferrite. *Phys. Rev. B.* **105**, 094102 (2022)
10. V.B. Shirokov, Y.I. Golovko, V.M. Mukhortov, Optical properties of BiFeO_3 epitaxial thin films. *Tech. Phys.* **59**, 102–106 (2014)
11. K. Karthikeyan, A. Thirumoorthi, BiFeO_3 -Montmorillonite intercalated nano composites – synthesis and its characterization. *Nanosyst. Phys. Chem. Math.* **9**(5), 631–640 (2018)
12. A. Feroze, M. Idrees, D.K. Kim, M. Nadeem, S.A. Siddiqi, S.F. Shaikat, M. Atif, M. Siddique, Low temperature

- synthesis and properties of BiFeO₃. *Electronic Mater.* **46**, 4582–4589 (2017)
13. A.V. Egorysheva, T.B. Kuvshinova, V.D. Volodin, O.G. Ellert, N.N. Efimov, V.M. Skorikov, A.E. Baranchikov, V.M. Novotortsev, Synthesis of high-purity nanocrystalline BiFeO₃. *Inorg. Mater.* **49**, 310–314 (2013)
 14. S.G. Nair, J. Satapathy, N.P. Kumar, Influence of synthesis, dopants, and structure on electrical properties of bismuth ferrite (BiFeO₃). *Appl. Phys.* **126**, 836 (2020)
 15. S. Xiao, A. Fakhri, B.J. Janani, Synthesis of spinel Tin ferrite decorated on Bismuth ferrite nanostructures for synergetic photocatalytic, superior drug delivery, and antibacterial efficiencies. *Surf. Interfaces.* **27**, 101490 (2021)
 16. P. Sharma, P.K. Diwan, O.P. Pandey, Impact of environment on the kinetics involved in the solid-state synthesis of bismuth ferrite. *Mater. Chem. Phys.* **233**(15), 171–179 (2019)
 17. K.S. Sivaraj, K.S. Sreehari, R.N. Bhowmik, M.R. Anantharaman, Sillénite phase stabilized ferromagnetic ordering in multiphase magnetoelectric bismuth ferrite. *J. Solid State Chem.* **299**, 122162 (2021)
 18. N.A. Liedienov, A.V. Pashchenko, V.A. Turchenko, V.Y. Sycheva, A.V. Voznyak, V.P. Kladko, A.I. Gudimenko, D.D. Tatarchuk, Y.V. Didenko, I.V. Fesych, I.I. Makoed, A.T. Kozakov, G.G. Levchenko, Liquid-phase sintered bismuth ferrite multiferroics and their giant dielectric constant. *Ceram. Int.* **45**(12), 14873–14879 (2019)
 19. K.P. Andryushin, V.P. Sakhnenko, A.V. Turik, L.A. Shilkina, A.A. Pavelko, S.I. Dudkina, A.G. Rudskaya, D.D. Rudskiy, I.A. Verbenko, S.V. Hasbulatov, L.A. Reznichenko, I.A. Parinov, S. Chang, H. Wang, Reasons for the high electrical conductivity of bismuth ferrite and ways to minimize it. *Appl. Sci.* **11**(3), 1025 (2021)
 20. T. Rojac, A. Bencan, B. Malic, G. Tutuncu, J.L. Jones, J.E. Daniels, D. Damjanovic, BiFeO₃ ceramics: processing, electrical, and electromechanical properties. *J. Am. Ceram. Soc.* **97**(7), 1993–2011 (2014)
 21. N.V. Srihari, K.B. Vinayakumar, K.K. Nagaraja, Magneto-electric coupling in bismuth ferrite-challenges and perspectives. *Coatings* **10**(12), 1221 (2020)
 22. S.R. Burns, O. Paull, J. Juraszek, V. Nagarajan, D. Sando, The experimentalist's guide to the cycloid, or noncollinear antiferromagnetism in epitaxial BiFeO₃. *Adv. Mater.* **32**(45), 2003711 (2020)
 23. A. Dubey, M.E. Castillo, J. Landers, S. Salamon, H. Wende, U. Hagemann, P. Gemeiner, B. Dkhil, V.V. Shvartsman, D.C. Lupascu, Effect of Mn and Ba codoping on a magnetic spin cycloid of multiferroic bismuth ferrite nanoparticles. *J. Phys. Chem.* **124**(40), 22266–22277 (2020)
 24. G. Dhir, N.K. Verma, Enhanced magnetization in Dy-doped bismuth ferrite nanoparticles. *AIP Conf. Proc.* **2220**, 020193 (2020)
 25. S.R. Dhanya, J. Satapathy, P. Kumar, A review on the structural and magnetic properties of differently doped bismuth-ferrite multiferroics. *Crystallogr. Rev.* **27**, 178–205 (2021)
 26. M.S. Bozgeyik, N. Kirkgecit, R.K. Katiyar, R.S. Katiyar, Monitoring structural variation on Gd ratio of La modified bismuth ferrite ceramics with enhanced magnetization. *J. Alloys Compd.* **819**, 153050 (2020)
 27. K.L. Da Silva, R.S. Trautwein, R.B. Da Silva, M. Fabián, E. Čížmár, M. Holub, O. Skurikhina, M. Harničárová, V. Girmán, D. Menzel, K.D. Becker, H. Hahn, V. Šepelák, Suppression of the cycloidal spin arrangement in BiFeO₃ caused by the mechanically induced structural distortion and its effect on magnetism. *Front. Mater.* **8**, 717185 (2021)
 28. I.I. Makoed, A.F. Revinskij, Osobennosti jevoljucii magnitnyh svojstv ferrita vismuta, modifirovannogo kationami redkozemel'nyh jelementov. *Fizika tverdogo tela.* **57**(9), 1742–1747 (2015)
 29. H.A. Sadykova, I.A. Verbenko, L.A. Reznichenko, A.G. Abubakarov, L.A. Shilkina, O.N. Razumovskaya, S.I. Dudkina, Kriticheskaya zavisimost' svojstv BST-keramik ot uslovij ih strukturoobrazovaniya. *Konstrukcii iz kompozicionnyh materialov.* **2**, 43–49 (2013)
 30. M. Yousaf, Y. Lu, E. Hu, B. Wang, M.N. Akhtar, A. Noor, M. Akbar, M.A.K.Y. Shah, F. Wang, B. Zhu, Tunable magneto-optical and interfacial defects of Nd and Cr-doped bismuth ferrite nanoparticles for microwave absorber applications. *J. Colloid Interface Sci.* **608**, 1868–1881 (2022)
 31. Y.J. Yoo, J.S. Hwang, Y.P. Lee, J.S. Park, J.-H. Kang, J. Kim, High ferromagnetic transition temperature in multiferroic BiFe_{0.95}Ni_{0.05}O₃ compound. *J. Appl. Phys.* **114**, 163902(2013)
 32. T.K. Pani, B. Sundaray, A correlation of lattice distortion with the magnetic properties of calcium doped bismuth ferrite thin films. *J. Phys. D: Appl. Phys.* **54**, 1 (2021)
 33. E.V. Tomina, I.Y. Mittova, O.V. Stekleneva, N.A. Kurkin, N.S. Perov, Y.A. Alekhina, Microwave synthesis and magnetic properties of bismuth ferrite nanoparticles doped with cobalt. *Rus. Chem. Bull.* **69**, 941–946 (2020)
 34. C.R. Joshi, M. Acharya, G.J. Mankey, A. Gupta, Effect of thickness and frequency of applied field on the switching dynamics of multiferroic bismuth ferrite thin films. *Phys. Rev. Mater.* **6**, 054409 (2022)
 35. E.V. Tomina, A.A. Pavlenko, N.A. Kurkin, Synthesis of bismuth ferrite nanopowder doped with erbium ions. *Condens. Matter Interphases.* **23**(1), 93–100 (2021)

36. X. Zhou, D. Bu, H. Liu, L. Deng, H. Liu, P. Yuan, P. Du, H. Song, XRD-based quantitative analysis of clay minerals using reference intensity ratios, mineral intensity factors, Rietveld, and full pattern summation methods: a critical review. *Solid Earth Sci.* **3**(1), 16–29 (2018)
37. S.G. Nair, J. Satapathy, N.P. Kumar, Effect of holmium (Ho) partial substitution in structure and ferroelectric properties of bismuth ferrites (BFO). *J. Alloys Compd.* **895**, 162599 (2022)
38. N. Sheoran, A. Kumar, V. Kumar, A. Banerjee, Structural, optical, and multiferroic properties of yttrium (Y^{3+})-substituted $BiFeO_3$ nanostructures. *J. Supercond. Nov. Magn.* **33**, 2017–2029 (2020)
39. Md.R. Islam, M.A. Zubair, R.H. Galib, MdSh. Bin Hoque, J.A. Tomko, K. Aryana, A.K. Basak, P.E. Hopkins, Vacancy-induced temperature-dependent thermal and magnetic properties of holmium-substituted bismuth ferrite nanoparticle compacts. *ACS Appl. Mater. Interfaces.* **14**(22), 25886–25897 (2022)
40. B.K. Hoang, V.O. Mittova, A.T. Nguyen, T.Y.D. Pham, Structural and magnetic properties of Ho-doped $CuFe_2O_4$ nanoparticles prepared by a simple co-precipitation method. *Condens. Matter Interphases.* **24**, 109–115 (2022)
41. T.A. Nguyen, V. Pham, T.L. Pham, I.Y. Mittova, V.O. Mittova, L.N. Vo, Simple synthesis of $NdFeO_3$ nanoparticles by the co-precipitation method based on a study of thermal behaviors of Fe (III) and Nd (III) hydroxides. *Cryst.* **10**(3), 219 (2020)
42. T.A. Nguyen, V.N.T. Pham, H.T. Le, D.H. Chau, V.O. Mittova, I.Y. Mittova, Crystal structure and magnetic properties of $LaFe_{1-x}Ni_xO_3$ nanomaterials prepared via a simple co-precipitation method. *Ceram. Intern.* **45**(17), 21768–21772 (2019)
43. C.P. Bean, J.D. Livingston, Superparamagnetism. *J. Appl. Phys.* **30**, S120 (1959)
44. I.R. Kayumov, K.A. Zvezdin, V. Gareeva, A.P. Pyatakov, A.K. Zvezdin, Spinovye cikloidy i konusnye modulirovannye struktury v (110)-epitaksial'nyh plenkah ferrita vismuta *Izvestiya RAN. Seriya fizicheskaya.* **83**(12), 1722–1725 (2019)
45. A. Franco, H.V.S. Pessoni, T.E.P. Alves, Enhanced dielectric permittivity on yttrium doped cobalt ferrite nanoparticles. *Mater. Lett.* **208**, 115–117 (2017)
46. A.V. Zhukov, S.V. Chizhevskaya, O.M. Klimenko, A.O. Merkushev, Glycine-nitrate synthesis of partially yttrium-stabilized zirconium nanopowders for hard ceramics. *Glass Ceram.* **70**, 400–403 (2014)
47. D.K. Palchaev, M.P. Faradzheva, S.A. Sadykov, M.H. Rabadanov, Zh.H. Murlieva, S.N. Kallaev, A.F.A. Tabit, R.M. Emirov, Osobennosti dielektricheskikh svoystv nanokristallicheskogo ferrita vismuta. *Pis'ma v ZHTEF.* **40**(21), 54–62 (2014)
48. K. Sreekanth, B. Dhanalakshmi, D. Madhavaprasad, Enhanced dielectric and magnetic properties of Cr/Co and Mn co-doped single phase multiferroic bismuth ferrite nanoparticles. *J. Indian Chem. Soc.* **99**, 100649 (2022)

Publisher's Note Springer Nature remains neutral with regard to jurisdictional claims in published maps and institutional affiliations.

Springer Nature or its licensor holds exclusive rights to this article under a publishing agreement with the author(s) or other rightsholder(s); author self-archiving of the accepted manuscript version of this article is solely governed by the terms of such publishing agreement and applicable law.